

Mechanical and Microstructural Characteristics of Ambient Cured Fly Ash-Based Geopolymer Materials

Dipankar Das ^{1,*} , Prasanta Kumar Rout ^{1,*} 

¹ Department of Material Science and Engineering, Tripura University (A Central University), Suryamaninagar, Agartala, Tripura-799022, India

* Correspondence: dipankar.msen@tripurauniv.in; prasantarout@tripurauniv.ac.in;

Scopus Author ID 57220885336

Received: 9.12.2024; Accepted: 10.03.2025; Published: 12.04.2025

Abstract: Aluminosilicate source powder and various alkaline solutions can be combined to produce three-dimensional eco-friendly materials known as geopolymers. Due to the presence of amorphous aluminosilicate phases, fly ash powder, a byproduct of a thermal power plant, has the potential to serve as a raw material for geopolymer synthesis. In this current investigation, geopolymers are prepared by alkali activation of fly ash powder with an alkaline solution. Geopolymer samples were synthesized using class F fly ash powder and a combination of 14 molar sodium hydroxide (NaOH) solutions and sodium silicate (Na₂SiO₃) solutions, followed by ambient curing. After curing, the mechanical properties, such as compressive strength, are determined. The specimen of geopolymer that has undergone a 390-day ambient curing process has the maximum compressive strength, flexural strength, and micro-hardness value of 89.47 MPa, 15.8 MPa, and 171.21 HV, respectively. To confirm mechanical properties data, tested samples were further analyzed by field emission scanning electron microscopy (FESEM) equipped with energy-dispersive X-ray spectroscopy (EDS), high-resolution transmission electron microscopy (HRTEM), X-ray diffraction (XRD) and Fourier transform infrared spectroscopy (FTIR), respectively. Further, to test the durability, a water absorption test was conducted where the immersion days were 7, 14, and 28 days, respectively. The lowest water absorption was 5.70% after exposure for 28 days.

Keywords: fly ash; industrial waste; environment; geopolymer; construction materials; waste.

Abbreviations: NH: Sodium hydroxide; NS: Sodium silicate; NTPC: National Thermal Power Corporation Limited; BgTPP: Bongaigaon thermal power plant; N-A-S-H: Na₂O-Al₂O₃-SiO₂-H₂O; C-A-S-H: CaO-Al₂O₃-SiO₂-H₂O.

© 2025 by the authors. This article is an open-access article distributed under the terms and conditions of the Creative Commons Attribution (CC BY) license (<https://creativecommons.org/licenses/by/4.0/>).

1. Introduction

Alkali-activated materials are gaining much more attention due to their synthesized techniques. They use industrial solid waste such as fly ash powder [1], red mud [2], ground granulated blast furnace slag [3], LD slag [4], zinc slag [5], chromium slag [6], ferrochrome slag [7], nickel slag [8], etc. which results in the environmental benefits. Due to urbanization and the electricity demand, coal utilization in coal-based thermal power plants is increasing daily to meet the issues. China is the top coal consumer in the world as of 2015. India is one of the major fly ash producers among the world's top ten fly ash producer countries. Between 2015 and 2035, India's coal consumption for its different coal-based thermal power plants

might double, from 407 to 833 mtoe (Millions of tonnes of oil equivalent) [9], which can result in more fly ash. Fly ash powders are one of the solid industrial wastes left behind after coal is burned in coal-based thermal power plants. After combustion, the particles that rise along with the flue gases are called fly ash, and the particles that do not rise and settle down at the bottom of the furnace are called bottom ash. The fine particles from the flue gases are removed by filtration or electrostatic precipitators. Fly ash's constituents vary significantly depending on the type of coal being burned as well as its origin and composition. It may contain a toxic element (Cr, Se, B, Pb, As, Cd, Ni, Sb, Zn, and Sn) that depends on the coal bed [10]. Two types of fly ash are available according to the ASTM C618, such as Class C and F type [11,12]. Fly ash powders are one of the major sources of aluminosilicate materials, making this industrial solid waste suitable for utilization in the field of geopolymer. An abundant amount of fly ash is generated globally annually, which results in various environmental issues such as air, surface water, groundwater, and soil pollution, respectively [13-16]. Also, vast areas are required for their disposal, so using these materials is gaining much more attention from researchers by utilizing geopolymer technology.

The aluminosilicate source materials can be activated by alkaline solutions, such as sodium or potassium hydroxide solutions, along with sodium or potassium silicate solutions. Researchers have done many works on alkali-activated materials, which possess excellent physical, mechanical, and durability properties in high-temperature conditions and acid medium, respectively. Two curing methods are mainly used to develop fly ash-based geopolymers' mechanical properties: ambient curing and high-temperature curing. The geopolymer process is complex, and it involves several steps. Due to alkaline activation, the dissolution of Al and Si takes place from the source materials and forms a geopolymer gel. The next step involves hydrolysis, which entails breaking the bond and enabling silicate and aluminate tetrahedral units to link with one another since water molecules are present. After that, polycondensation occurs and forms an aluminosilicate network [17]. Sodium aluminosilicate hydrate gel (N-A-S-H) is the primary reaction product for fly ash-based geopolymers, mainly responsible for forming mechanical characteristics [18,19].

Geopolymer concrete under ambient curing was studied by Rahman *et al.* [20], where the raw materials were fly ash, micro fly ash, and slag. The increase in ambient curing days was reported to enhance the compressive strength, where the highest compressive strength of 45 MPa was achieved. Verma *et al.* [21] studied the impact of NaOH on the mechanical characteristics of a geopolymer based on fly ash and slag, where the specimen achieved the highest compressive of 25 MPa under ambient curing of 56 days. Ambient cured fly ash-based geopolymer prepared with only NaOH is studied by Somna *et al.* [22]. The compressive strength increases with the increment of NaOH concentration, and the maximum compressive strength of 25.5 MPa was attained after curing for 60 days with the NaOH concentration of 14 molars. Fly ash-based geopolymer concrete was prepared with 8 M, 10 M, 12 M, 14 M, and 16 M, respectively [23]. The increase in the concentration of geopolymer specimens from 8 M to 14 M enhances the mechanical properties, but after 14 M, the mechanical strength shows a reverse direction. The highest compressive strength of 39.67 MPa was achieved within 28 days of curing. Mudgal *et al.* [24] studied the geopolymer prepared with fly ash and red mud cured under ambient curing conditions. a maximum compressive strength of 65 MPa within 28 days of curing. One part of an alkali-activated fly ash-based geopolymer specimen was studied by Masi *et al.* [25] under ambient curing and artificial curing, respectively. The specimens cured

for 28 days under ambient curing show a compressive strength of 60 MPa. Ceramic waste and fly ash-based geopolymer concrete were studied by Bhavsar *et al.* [26] under ambient curing. It was reported that replacing 15% fly powder with ceramic waste powder shows excellent mechanical properties, such as compressive strength of 35 MPa to 45 MPa under ambient curing for 56 days. The ambient curing temperature was $35\pm 2^\circ\text{C}$. The formation of C-A-S-H gel with an N-A-S-H gel was confirmed by FESEM and XRD analysis, which was mainly responsible for mechanical strength development. Niş *et al.* [27] studied the slag and fly ash-based geopolymer, where different compositions were proposed. It was observed that the specimens that are cured for 28 days and 90 days show the highest compressive strength.

Many researchers have reported that curing conditions and age (days) play an important role in improving the mechanical properties of geopolymer specimens. Various researchers have also reported that higher curing temperatures accelerate the geopolymerization process of fly ash-based geopolymer and form the gel, which further results in excellent mechanical properties. Geopolymer materials are termed green materials, but when we apply the external curing process, they consume high energy and result in CO₂ emission to the environment. Very limited studies on the long-term curing of geopolymer specimens have been reported. The current study aims to utilize fly ash to develop geopolymer specimens, where the specimens are cured under ambient conditions. The geopolymer specimens' curing ages (days) are 3, 30, 90, 150, 210, 270, 330, and 390 days, respectively. After ambient curing, the cured specimens are tested using the universal testing machine for mechanical properties such as compressive strength, flexural strength, and Vickers microhardness tester for the hardness value of the geopolymer specimen. The fractured specimens are characterized by using field emission scanning electron microscopy (FESEM) equipped with energy-dispersive X-ray spectroscopy (EDS), high-resolution transmission electron microscopy (HRTEM), X-ray diffraction (XRD) and Fourier transform infrared spectroscopy (FTIR), respectively. The water absorption test was also conducted to check the durability of the geopolymer specimens, followed by a residual compression test and FESEM analysis.

2. Materials and Methods

The fly ash powder from NTPC BgTPP was used to synthesize the geopolymer specimen. A thorough characterization of the as-received fly ash has been previously published by Das *et al.* [28]. The alkaline activators NH in the form of flakes with a minimum purity level of 97 % and NS solutions with the composition of SiO₂ and Na₂O of 25-28% and 7.5-8.5% are purchased from LOBA Chemie Private Limited (India). The flakes of NH are mixed with distilled water at an appropriate weight. The concentrations of NH were maintained at 14 molars, which was chosen on the basis of a literature study [29,30]. Since the mixing process of adding NH flake in distilled water produces heat, the prepared NH solutions of the desired concentration are kept at room temperature for 24 hours to obtain a stable and homogeneous mixture. The combination of NH and NS was used to synthesize the specimen, where the ratio of NS/NH was 1, and the ratio of liquid to solid was 0.3. The fly ash powder was first mixed with NH solutions, followed by adding NS solutions manually for 3 to 5 minutes. The fly ash and alkaline solutions are mixed in a jar, and the pastes are cast in the mold and kept at room temperature for 24 hours. After 24 hours, the specimens are demolded from the mold and cured under ambient conditions ($24\pm 5^\circ\text{C}$) for various days, such as 3, 30, 90, 150, 210, 270, 330, and 390 days. The cured specimens are tested under universal testing machine. The experimental procedure for synthesis of geopolymer specimens is depicted in Figure 1's flow chart and the

detail mix designs of geopolymer paste are tabulated in Table 1. Table 2 shows the geopolymer samples ID before and after curing.

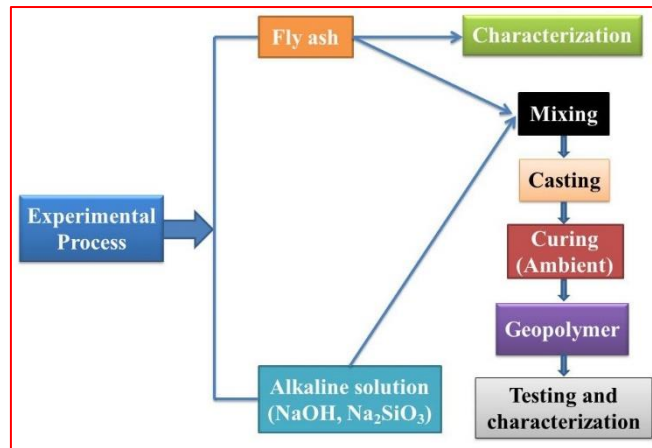


Figure 1. Flow chart of experimental process of geopolymer specimen preparation.

Table 1. Mix design of geopolymer paste for natural curing specimen.

Sl. No.	Sample ID	Raw materials	Molarity (M) of NaOH solution	Na ₂ SiO ₃ solution/NaOH solution ratio	Liquid (activator)/ Solid (Fly ash powder) ratio	Curing condition and time
1	GP14MAC	Fly ash	14	1	0.3	Curing condition: Room temperature (24±5°C) and curing time: 3 days, 30 days, 90 days, 150 days, 210 days, 270 days, 330 days, 390 days

Note: GP14MAC indicates a geopolymer prepared with 14 molar NaOH and Na₂SiO₃ solutions.

Table 2. Descriptions of geopolymer samples ID before and after curing.

Sl. no.	Sample ID (Before curing)	Curing age (days)	Sample ID (After curing)
1	GP14MAC	3	GP14MAC3D
2	GP14MAC	30	GP14MAC30D
3	GP14MAC	90	GP14MAC90D
4	GP14MAC	150	GP14MAC150D
5	GP14MAC	210	GP14MAC210D
6	GP14MAC	270	GP14MAC270D
7	GP14MAC	330	GP14MAC330D
8	GP14MAC	390	GP14MAC390D

Note: Sample ID GP14MAC3D, GP14MAC30D, GP14MAC90D, GP14MAC150D, GP14MAC210D, GP14MAC270D, GP14MAC330D, GP14MAC390D indicate a geopolymer prepared with a 14 molar NaOH; Na₂SiO₃ solutions followed by cured under ambient condition for 3, 30, 90, 150, 210, 270, 330, and 390 days, respectively.

3. Result and Discussions

The color of the source materials is light grey. The density of the received fly ash powders is 0.85 g/cm³ (bulk density) and 2.1 g/cm³ (true density), respectively. The chemical compositions of the as-received source materials are listed in Table 3. It is clear from the table that SiO₂ and Al₂O₃ are the main constituents of the source materials, and there are also other minor constituents like CaO, Fe₂O₃, TiO₂, and MgO, respectively. SiO₂ and Al₂O₃ together make up 85.4 % of the material, where the percentage of CaO is 1.59 %, which shows that the as-received source materials come under the type of class F fly ash as per ASTM C618 [31-33].

Table 3. Major chemical compositions (%) of fly ash powder.

Sl. No.	Oxides	FA powder (%)
1	SiO ₂	55.60
2	Al ₂ O ₃	29.80
3	CaO	1.59
4	Fe ₂ O ₃	5.91
5	TiO ₂	1.63
6	MgO	1.08

SEM micrographs of as-received raw fly ash powders are shown in Figure 2, which was observed by using the Carl Zeiss make Sigma 300 FESEM equipped with EDS. To analyze the powder samples, the powders are coated with gold (Au) with a sputter coater. The micrograph (Figure 2a, 2b) shows that most of the particles are spherical. All the particle's size is less than 100 microns. Along with spherical particles, a few non-spherical, irregular, and angular particles are observed. The agglomeration of fly ash particles is also seen in Figure 2(a,b). A porous particle of size ranges 15 to 65 microns is present in Figure 2(b).

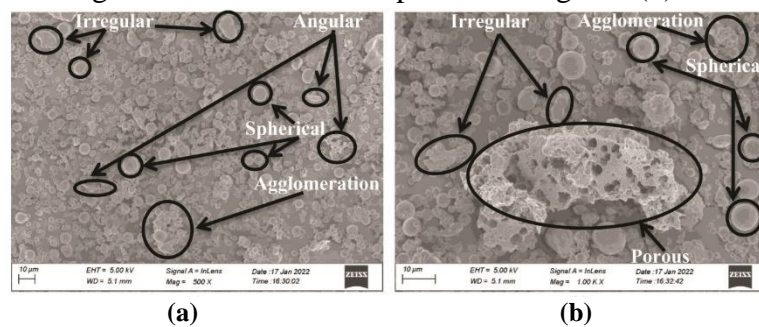


Figure 2. Representative SEM images of raw fly ash powder.

EDS spectra of porous particles marked in Figure 2(b) are shown in Figure 3. The porous particle contains various elements such as C, Ti, O, Fe, Al, Si, and Fe, respectively. From elemental tables, it can be observed that the maximum amount of the element present in this is carbon (C). The weight % of C, O, Al, Si, Ti, Fe, and Au is 49.93%, 21.37%, 5.03%, 8.06%, 0.94%, 0.98%, and 13.69%, respectively. Fly ash with significant levels of unburned carbon generally has lower market demand. The presence of more carbon particles (38.8%) in the fly ash reduces its use for Portland cement concrete as per ASTM C618 [34]. However, poorly controlled coal combustion processes may cause a lot of unburned carbon production in the fly ash. Unburned carbon can slow down reactions by absorbing alkaline solutions, impede the precursor's ability to dissolve, and reduce the workability of the paste [34,35]. The presence of gold (Au) in the EDS spectra (Figure 3) is due to the coating of gold on the particle surface, which improves the conductivity of the fly ash particles.

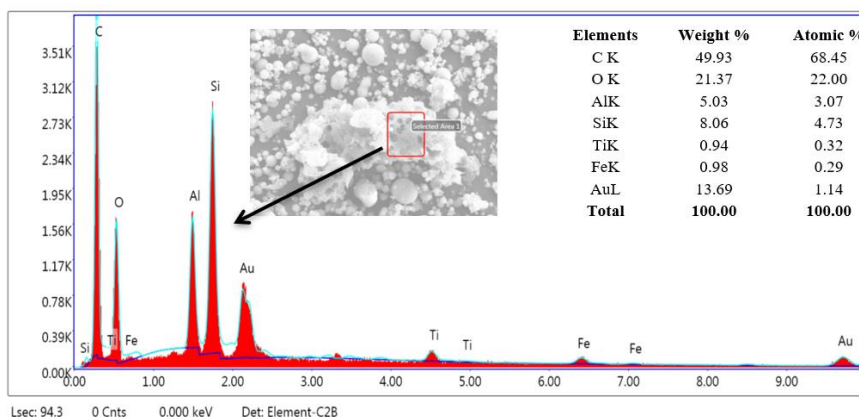


Figure 3. EDS spectra of porous particles marked in Figure 2(b).

The elemental mapping of raw fly ash powder is shown in Figure 4, where Figures 4(a-i) show the electron image in BSE mode, Si distribution, Al distribution, Ca distribution, Fe distribution, Ti distribution, Mg distribution, Mn distribution, and O distribution, respectively. It displays about eight elements (Si, Al, Ca, Fe, Ti, Mg, Mn, O) in the corresponding area of mapping. The color indicates the presence of single elements on the surface. Figure 4 shows that the presence of Si, Al, and O elements on the surface is greater than that of the other elements.

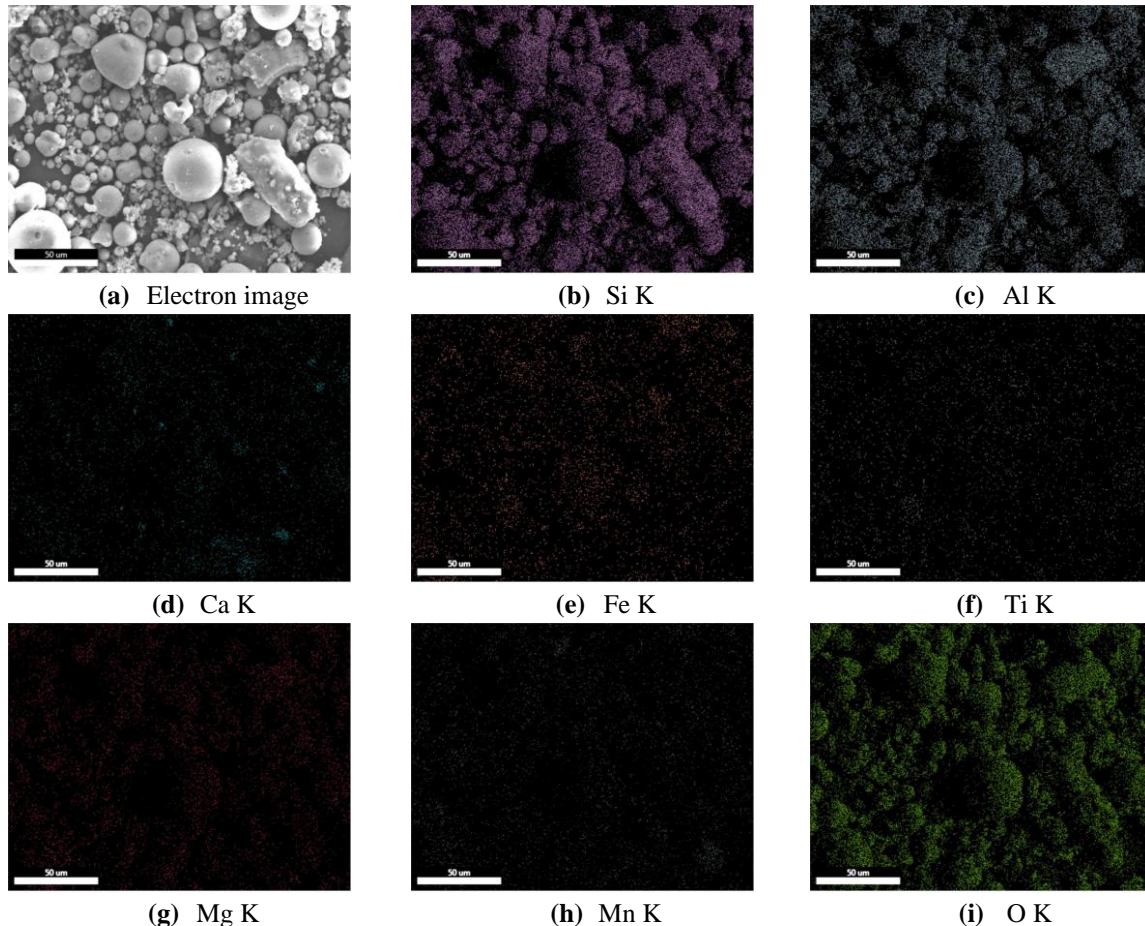


Figure 4. SEM and element mapping of fly ash powder (a) SEM micrograph in BSE mode; (b) Si distribution; (c) Al distribution; (d) Ca distribution; (e) Fe distribution; (f) Ti distribution; (g) Mg distribution; (h) Mn distribution; (i) O distribution.

The bulk density and shrinkage of ambient cured geopolymer specimens are shown in Table 4. By dividing the specimen's mass by its volume, the bulk densities of geopolymer specimens are determined. The highest bulk density of geopolymer is 2.01 g/cc, achieved by the specimen ambient cured for 390 days. The drying shrinkage (%) of geopolymer specimens is calculated by using the formula:

$$\text{Drying shrinkage}(\%) = \frac{(D_i - D_f)}{D_i} \times 100$$

Where D_i is the initial diameter of the specimen, D_f is the final diameter of the geopolymer specimen. From the drying shrinkage (%) data in Table 4, it can be observed that with the increase of curing age (days), the shrinkage (%) increases due to the water loss of the geopolymer specimen during the drying process. A minimum of three specimens were taken for the calculation of bulk density, and the shrinkage of geopolymer specimens and their average were reported.

Table 4. Bulk density (g/cc) and shrinkage (%) of the geopolymer specimens.

Sl. no.	Sample ID	Bulk density (g/cc)	Drying shrinkage (%)
1	GP14MAC3D	1.90	0.81
2	GP14MAC30D	1.93	0.89
3	GP14MAC90D	1.95	0.97
4	GP14MAC150D	1.95	1.00
5	GP14MAC210D	1.98	1.21
6	GP14MAC270D	1.99	1.43
7	GP14MAC330D	2.00	1.49
8	GP14MAC390D	2.01	1.50

The development of mechanical properties is being studied as an ongoing experiment for up to 390 days. The mechanical properties such as compressive strength, flexural strength, and Vickers microhardness value of geopolymeric specimen ID GP14MAC cured under ambient conditions (room temperature- $24\pm 5^{\circ}\text{C}$) for various days such as 3 days, 30 days, 90 days, 150 days, 210 days, 270 days, 330 days, and 390 days are plotted in Figure 5.

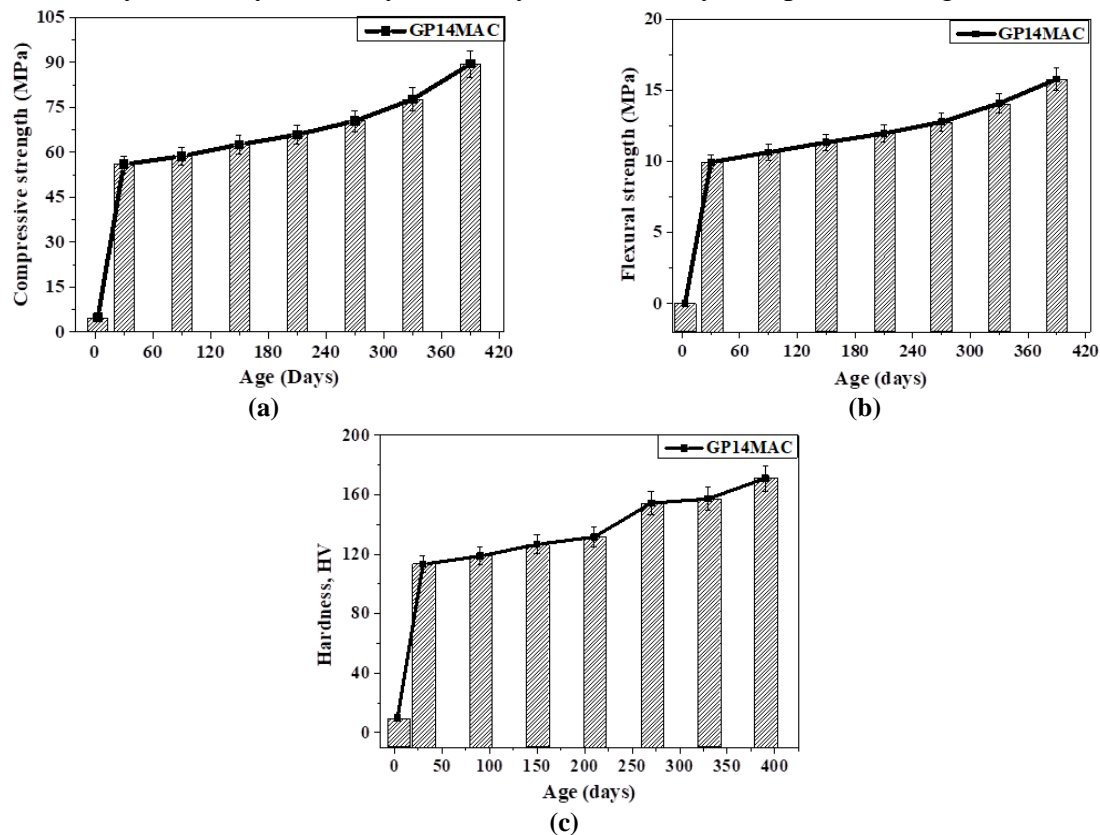


Figure 5. Mechanical properties of geopolymer specimens after ambient curing: (a) compressive strength; (b) flexural strength; (c) hardness.

At least three specimens are tested for reproducibility, and their average values are reported. Figure 5 shows that with the increase in curing days, the mechanical properties of geopolymer specimens are enhanced, which implies that curing time plays an important role in strength development. The specimen which is cured for 3 days shows a compressive strength of 4.86 MPa, and the specimen cured for 30 days, 90 days, 150 days, 210 days, 270 days, 330 days, and 390 days shows a compressive strength of 55.93 MPa, 58.66 MPa, 62.53 MPa, 65.86 MPa, 70.43 MPa, 77.66 MPa, and 89.47 MPa respectively. The maximum flexural strength of a geopolymer specimen cured for 390 days is 15.8 MPa. The Vickers microhardness values of geopolymer specimens are taken on the leveled exposed surface prepared by emery paper. The geopolymer specimen, cured for 3 days, shows the lowest Vickers microhardness value of 9.89

HV and cured for 390 days, which shows the highest Vickers microhardness value of 171.21 HV, respectively. Sodium aluminosilicate hydrate gel (N-A-S-H) is the main reaction product for fly ash-based geopolymers, which results in mechanical properties [36].

Cai *et al.* [37] studied the fly ash, slag, and metakaolin-based geopolymer, where the potassium hydroxide was used as an alkaline activator. It was observed that the geopolymer specimen cured under ambient curing conditions for 28 days increased the compressive strength. The fly ash and GGBFS-based geopolymer concrete was investigated under ambient curing by Nath *et al.* [38]. The mechanical properties, such as the compressive strength of the geopolymer concrete specimen, were tested after the ambient curing age of 28 days and 90 days, respectively. The geopolymer concrete specimen, which was cured for 28 days and 90 days, shows a compressive strength of 25-46 MPa and 53 MPa, respectively. The increment of strength is due to the addition of GGBFS, which ascribes to the formation of the C-S-H gel and the N-A-S-H gel. The flexural strength of concrete specimens also increased, similar to the compressive strength trend. However, adding up to 10% GGBFS shows an increase in flexural strength, which shows reverse trends after that. Vijai *et al.* [39] studied the effects of curing methods, such as ambient and hot curing, on fly ash-based geopolymer specimens. The specimen that was cured under ambient curing showed an increase of compressive strength after 7 days to 28 days, but for the hot air oven-cured specimen, the strength did not increase after 7 days. Hassan *et al.* [40] studied the fly ash-based geopolymer concrete, where the specimen was cured under ambient curing and heat cured for 26 hours at 75°C. It was reported that the temperature and curing process is important in the geopolymerization process. The increase in curing age increases the geopolymer specimen's compressive strength and flexural strength. Shekhawat *et al.* [41] studied the fly ash and egg shell based geopolymer, where the specimen was cured under ambient curing for 7, 28, and 56 days. The highest compressive strength of 2149 kPa was achieved with the specimen FA50:ESP50 (Fly ash 50: Egg shell powder 50) specimen.

A few representative SEM micrographs of fractured geopolymer specimens ID GP14MAC after compression testing are shown in Figure 6, Figure 7, Figure 8, and Figure 9, respectively. Geopolymer specimens are nonconductive in nature, which can result in the surface of the materials to act as an electron trap. When the electron beam from the electron gun hits the non-conducting nature specimen, it accumulates electrons on the surface, which is called “charging”. It also creates extra white regions on the specimen's SEM image. So before loading to the FESEM instrument, the geopolymer specimens are coated with (gold) to improve their conductivity. The image instability and arching during the image collection can be eliminated by gold (Au) coating, which improves the conductivity of the specimen surface. Figure 6 (a,b,c) shows the micrographs of fractured specimens cured for 3 days. From Figure 6, it can be observed that few particles are defused and start forming N-A-S-H gel due to high alkaline activation. Most particles do not participate in the geopolymerization process due to less activation curing time. A significant amount of fly ash is still present. Few unreacted, partially reacted particles and micro-cracks, along with geopolymer gels, can also be observed in the fractured specimen. The reaction mechanism of the source materials by high alkaline solution is very slow due to the less curing time and temperature, which results in low mechanical strength. Figure 6(c) shows that the starting raw materials, i.e., fly ash powders, are covered with sodium aluminosilicate gels.

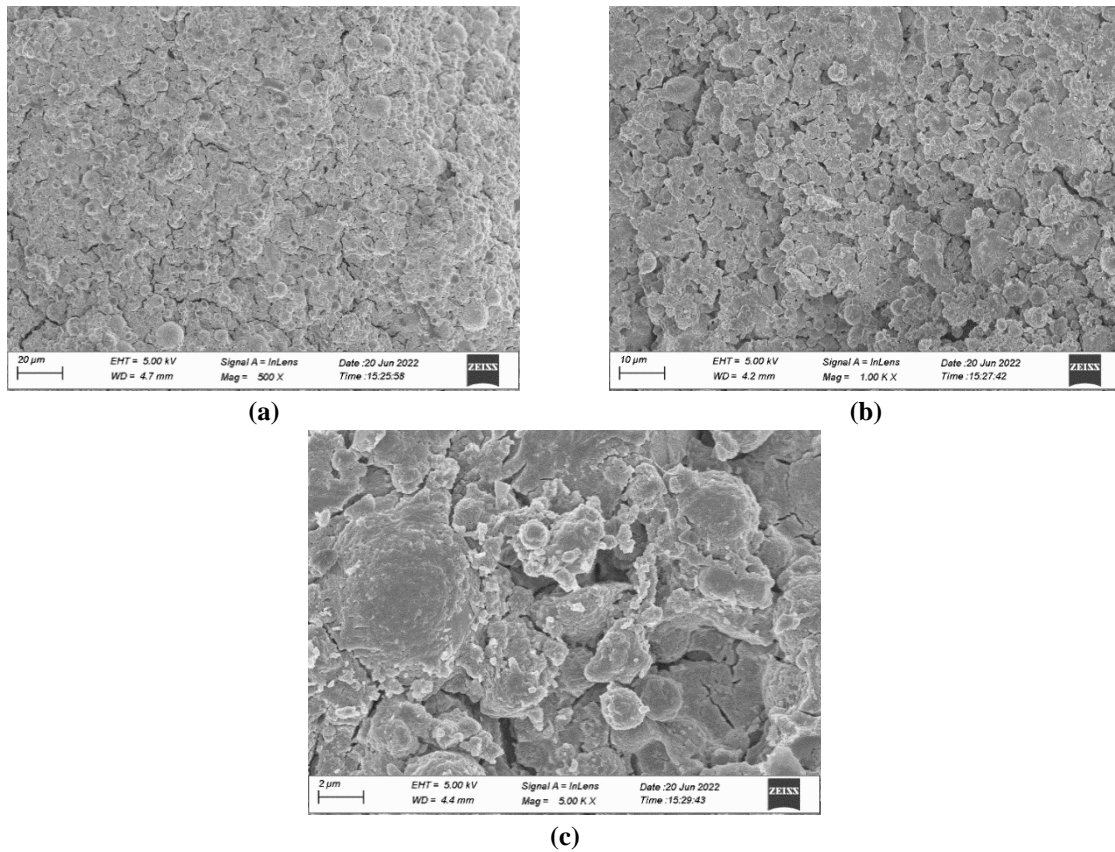


Figure 6. (a-c) FESEM fractograph of geopolymer specimen cured for 3 days under ambient curing.

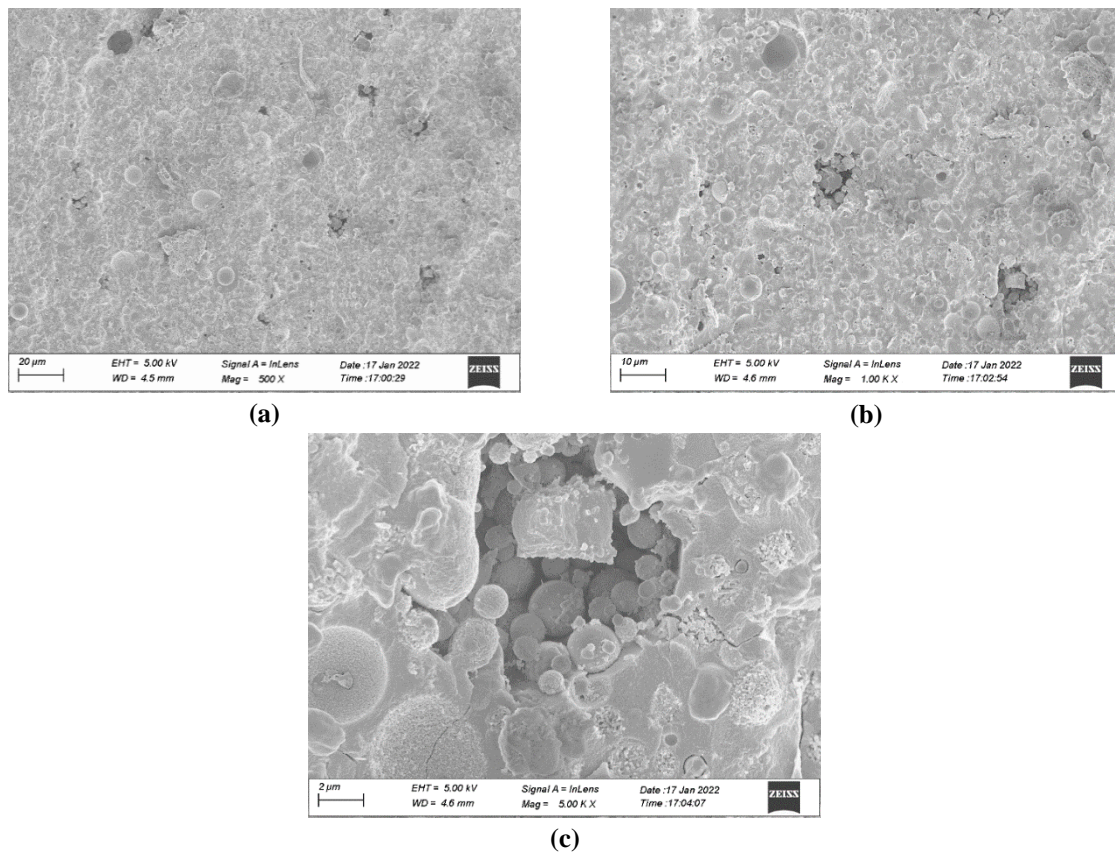


Figure 7. (a-c) FESEM fractograph of geopolymer specimen cured for 30 days under ambient curing.

Figure 7 (a-c) shows the FESEM fractograph of a geopolymer specimen cured for 30 days under ambient curing. In contrast to the geopolymer specimen that was cured for three days (Figure 6), it is evident from the fractograph that most of the particles reacted. A few

unreacted particles, partially reacted particles, pores, and micro-cracks can also be observed. Figure 7(c) shows a few unreacted, partially reacted particles and fly ash powder covered with geopolymer gel.

Figure 8 (a-c) elaborates the FESEM fractograph of geopolymer specimen cured under ambient curing conditions for 330 days. Figure 8(a-b) elaborates that very few undissolved, partially dissolved, and fully dissolved particles can be observed through the action of a highly alkaline solution along with cracks on the surface. Pores generated due to absorbed air in the specimen can also be observed. Figure 8(c) shows the aluminosilicate hydrate gel and compact structure.

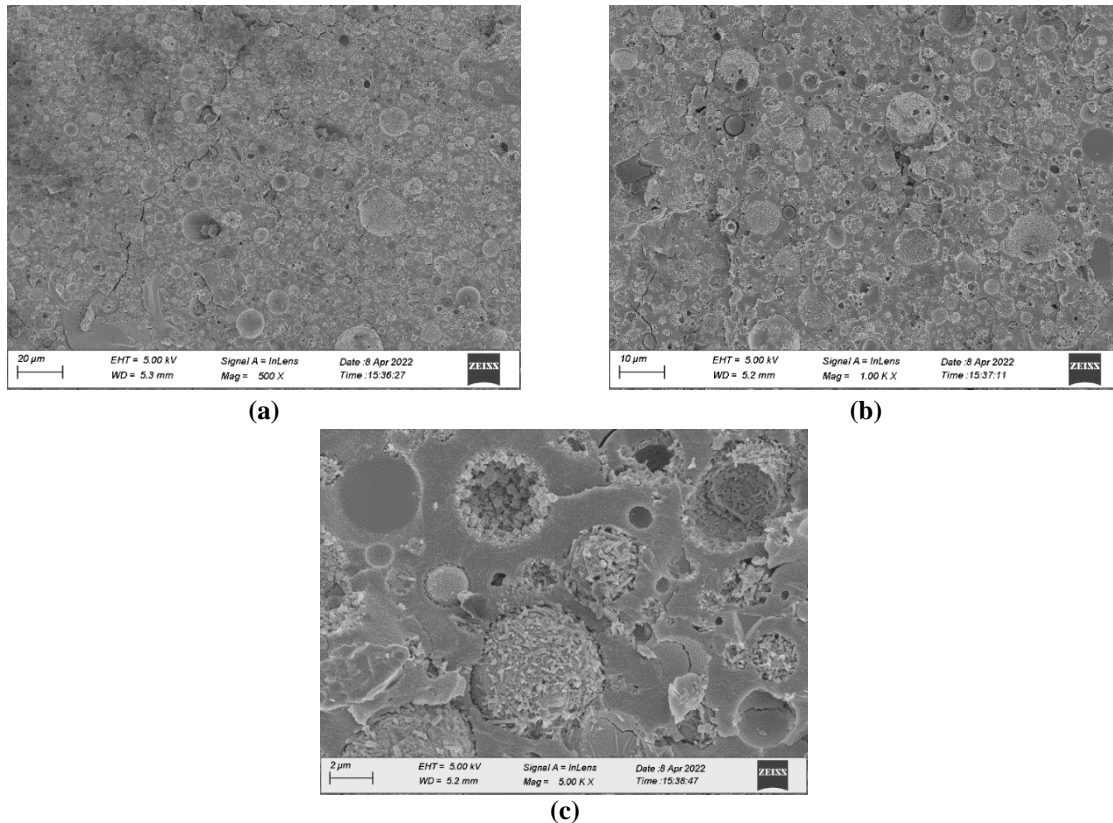


Figure 8. (a-c) FESEM fractograph of geopolymer specimen cured for 330 days under ambient curing.

Figure 9(a-c) shows the micrographs of the geopolymer specimen, which was cured in ambient curing conditions for 390 days. Figure 9(a-b) shows that most of the particles participated in the geopolymerization process due to more curing time than Figures 6, 7, and 8, respectively. Few unreacted particles are observed, along with few pores, micro-cracks, etc. The curing time plays an important role in the geopolymerization process, which results in strength development. The formation of N-A-S-H gel and its solidification results in a hardened, compacted structure that is responsible for excellent mechanical strength. The amorphous components of the fly ash particles are mostly dissolved, leaving behind needle or rod-like crystal phases typical of mullite and quartz, which can be observed in Figures 8(c) and 9(C). Identifying needle or rod-like features is consistent with other researchers' findings [42-44]. Bhavsar *et al.* [26] also observed a needle-like structure on the surface of the particles, where the size of the needles is 2 μm.

Energy dispersive X-ray spectroscopy of fly ash-based geopolymer specimens cured under ambient curing of 3 days, 30 days, 330 days, and 390 days, respectively, are shown in Figure 10(a-d). The EDS graph of the geopolymer specimen shows the presence of various major elements in the geopolymer specimen.

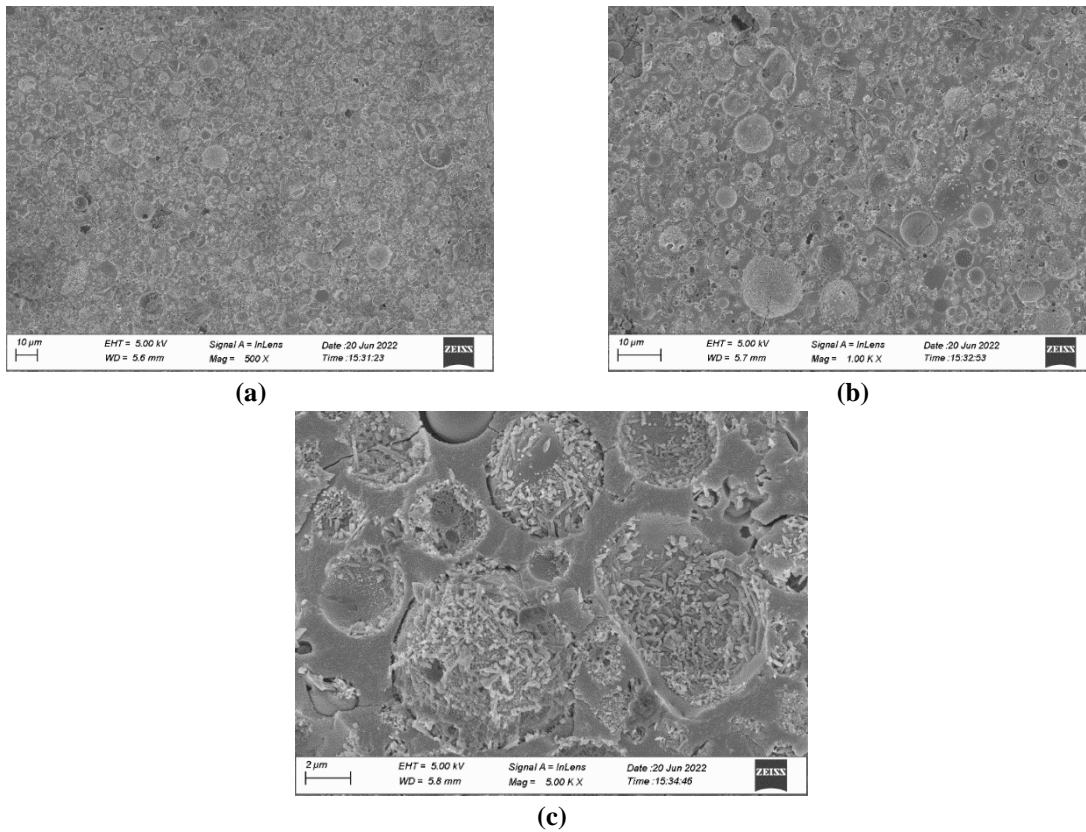
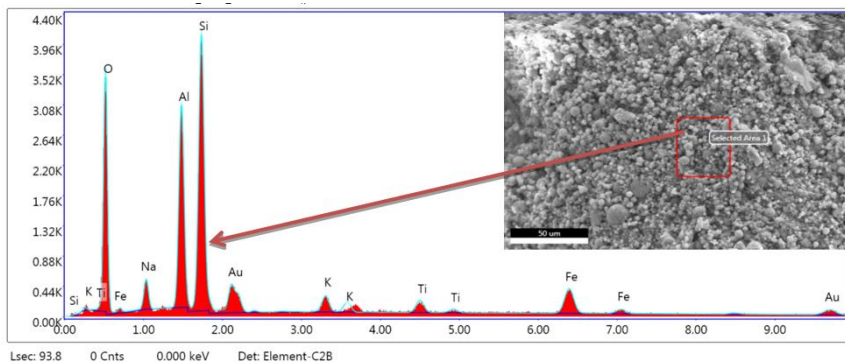
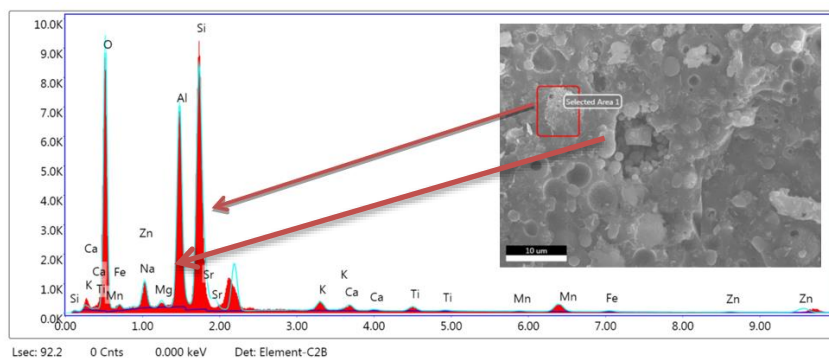


Figure 9. (a-c) FESEM fractograph of geopolymer specimen cured for 390 days under ambient curing.

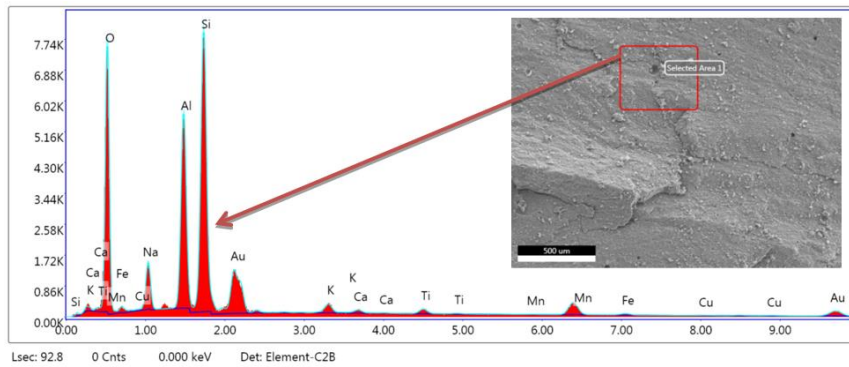
From the graph, we can observe that Si, Al, Na, and O are the major elements that are present, which implies that the formation of sodium aluminosilicate hydrate (N-A-S-H) gel in the geopolymer gel, which was also observed by other researchers also [45-48]. The formation of this gel results in the mechanical characteristics of the geopolymer specimen. Table 5 lists the major element details from the EDS spectra of one selected area of geopolymer specimen ID GP14MAC, which was cured for 390 days.



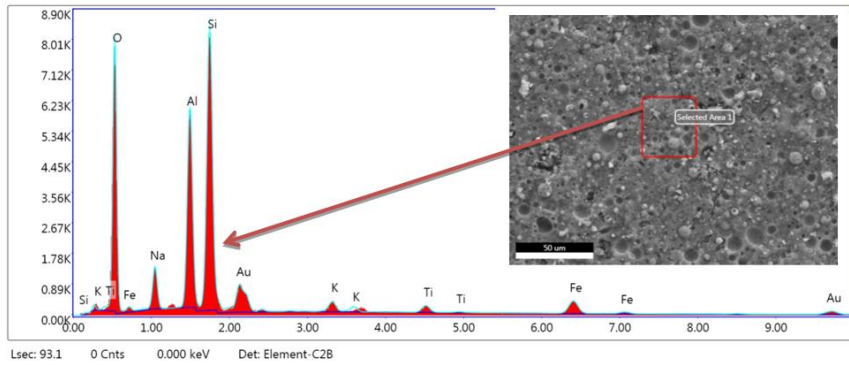
(a)



(b)



(c)



(d)

Figure 10. EDS spectra of geopolymer specimen cured under ambient curing for (a) 3 days; (b) 30 days; (c) 330 days; (d) 390 days, respectively.

The fly ash powder shows low reactivity under ambient temperature, but sufficient curing age (days) dissolves maximum fly ash particles and forms a hardened matrix. It can be observed that the weight % of elements, namely Si and Al, are increased with the curing time (days), which implies that more N-A-S-H gel forms with curing age (days), resulting in excellent mechanical properties.

Table 5. Element details from EDS spectra of geopolymer specimen.

Sl. no.	Specimen ID	EDS Figure No.	Major elements	Weight %	Atomic %
1	GP14MAC3D	Figure 10(a)	Na	3.57	3.98
			Al	14.67	13.07
			Si	20.44	18.22
			Fe	6.98	3.13
2	GP14MAC30D	Figure 10(b)	Na	4.92	4.83
			Al	15.02	13.52
			Si	20.90	16.24
			Fe	2.59	1.01
3	GP14MAC330D	Figure 10(c)	Na	6.78	7.10
			Al	15.71	13.94
			Si	21.18	18.13
			Fe	3.44	1.48
4	GP14MAC390D	Figure 10(d)	Na	6.53	6.57
			Al	16.55	14.34
			Si	22.64	18.65
			Fe	3.70	1.53

In order to see the distribution of elements on the GP14MAC390D geopolymer specimen, the fractured geopolymer specimens are analyzed through SEM analysis. The electron images of geopolymer specimens are shown in Figure 11(a), and the mapping results of geopolymer specimens are shown in Figure 11(b-j), respectively. The major distributions of

elements on the geopolymer surface are Si, Al, Na, and O, respectively. It can be observed that the distribution of Si, Al, and Na elements is near to homogeneous distribution. So, the main reaction product for the geopolymer specimen is the resulting bonding of Na, Al, and Si atoms, respectively, which implies the formation of N-A-S-H gel over the surface of the geopolymer specimen. The formation of these gels resulted in the mechanical properties of the specimen. Similar results are also observed by Somna *et al.* [22]. Azimi *et al.* [49] studied the fly ash and dolomite-based geopolymer composites under elevated temperature, where it was reported that the distributions of elements in the geopolymer composites are homogeneous and the presence of Na, Si, Al, and Ca elements C-(N)-A-S gel. It was also reported that one of the most significant linkages that affected the strength of the geopolymer was Si-O-Al, which was demonstrated by the combination of Si and Al maps. Kränzlein *et al.* [50] studied the fly ash-based geopolymer foam.

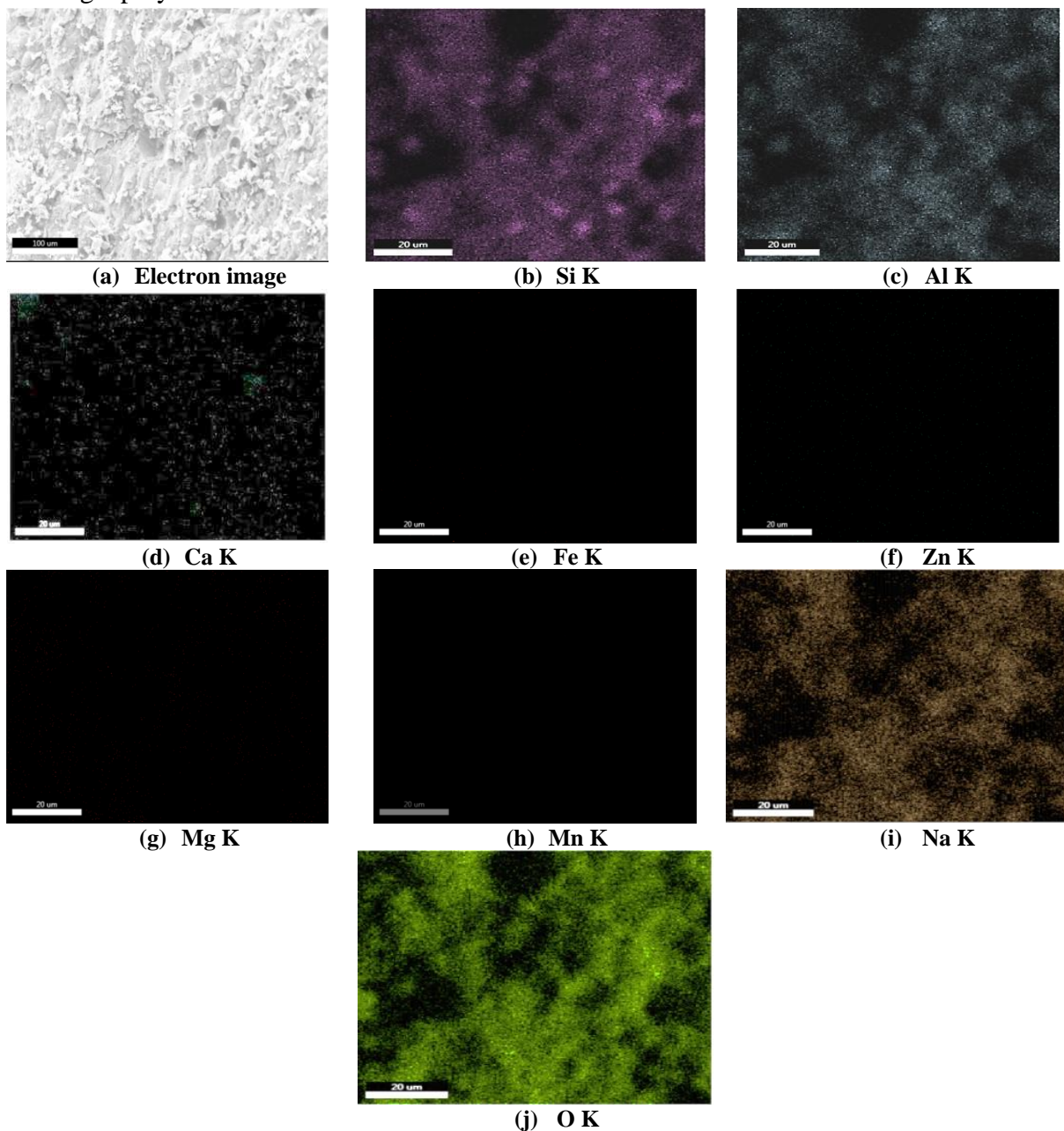


Figure 11. SEM and element mapping of geopolymer specimen ID GP14MAC390D: (a) SEM micrograph in BSE mode; (b) Si distribution; (c) Al distribution; (d) Ca distribution; (e) Fe distribution; (f) Zn distribution; (g) Mg distribution; (h) Mn distribution; (i) Na distribution; (j) O distribution.

The elemental mapping shows the few unreacted fly ash powders and the needle-shaped crystals due to more Na^+ ions in the geopolymer specimen. It was also reported that geopolymer gel (C, N)-A-S-H has been developed, which was observed by the element distribution of the gel phase. Shekhawat *et al.* [51] studied the fly ash and eggshell powder-based geopolymer specimens. The presence of Na, Ca, Si, Al, and O element distribution in the geopolymer specimen is higher as compared to the other elements, which represents the formation of bonding between the Na, Al, and Si atoms forms the geopolymerization product along with the formation of C-S-H gel in a small amount. Both the gel co-exist with each other and form a hybrid gel. Kumar *et al.* [52] developed the red mud and fly ash-based geopolymer paving blocks. The main constituent of red mud is Fe, so the mapping of the geopolymer specimen shows the Fe elements. It was reported that Fe is distributed in two ways: the Fe is embedded in the geopolymer gel, and the other is distributed in a few locations of the specimen.

Transmission electron microscopy was used to look more closely at the geopolymer sample's microstructural characteristics. Figure 12(a-b) displays the distinctive transmission electron microscopy bright field (BF) image and selection area electron diffraction (SAED) pattern of the geopolymer sample with the identification code GP14MAC390D. The activation of fly ash powders with an alkaline activator of NaOH, along with Na_2SiO_3 solutions, forms a geopolymer gel. The lighter part in Figure 12(a) is the N-A-S-H gel, and the darker parts are the dense, compacted geopolymer matrix. Other researchers have also confirmed the formation of geopolymer gel [53,54]. The whitened part in the HRTEM images of the geopolymer specimen GP14MAC390D is the porosity.

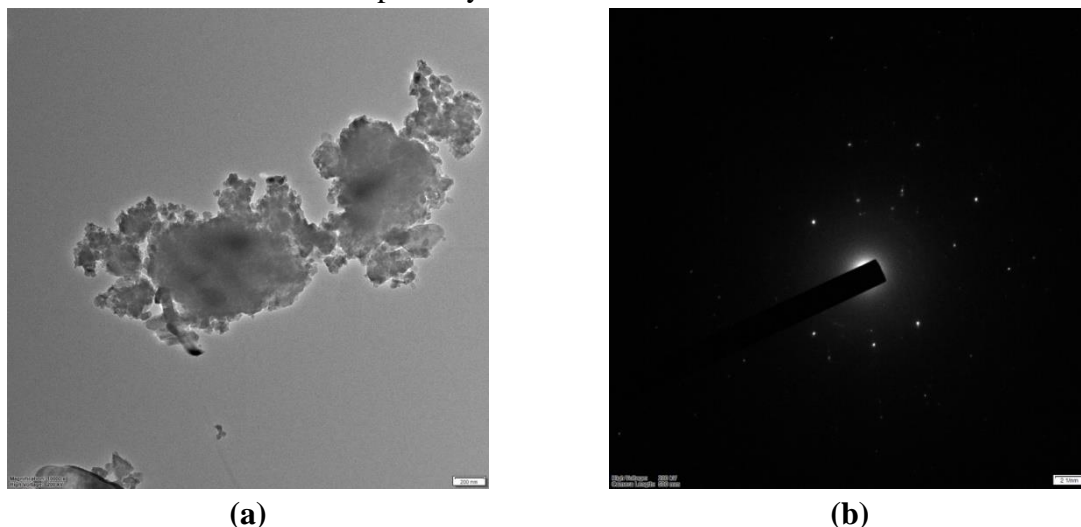


Figure 12. Transmission electron microscopy bright field (BF) image (a) and selection area electron diffraction (SAED) pattern (b) of geopolymer specimen ID GP14MAC390D.

Al-O and Si-O bonds in aluminosilicate source materials can be revealed at the atomic level with great accuracy using Fourier transform infrared spectroscopy (FTIR). Figure 13 shows the FTIR spectra of fly ash powders and the geopolymer specimen, which shows maximum compressive strength. Pu *et al.* [55] depict FTIR spectra into two primary spectrum sections, such as the high-frequency region, where the wavenumbers range from 400 cm^{-1} to 1400 cm^{-1} , and the low-frequency region ranges from 1400 cm^{-1} to 4000 cm^{-1} . The spectra of asymmetric stretching vibrations of Si-O-T (T= Tetrahedral Si or Al) show at 1071 cm^{-1} in fly ash powders, whereas in geopolymer specimen ID GP14MAC390D cured under ambient curing condition for 390 days shows the intense peak at 1085 cm^{-1} . The characteristic band in the 900 cm^{-1} to 1300 cm^{-1} ranges is subjected to the asymmetric stretching vibrations of Si-

O-Si or Si-O-Al [55-57]. Due to alkaline activation, the peak of fly ash at 1071 cm⁻¹ shifted to 1085 cm⁻¹, which implies that some chemical changes occurred in the structure and formed three-dimensional geopolymeric structures. One additional peak at 562 cm⁻¹ that represents the symmetric stretching of Al-O-Si after the geopolymerization process is seen in the geopolymer product but was not particularly noticeable in the fly ash powder. Another two intense peaks of the geopolymer specimen at 1645 cm⁻¹ and 3433 cm⁻¹ ascribe the bending vibrations of H-O-H and stretching vibrations of OH, respectively. The weak peak at 1645 cm⁻¹ is a result of the water molecules being absorbed, causing H-O-H bending vibrations. The presence of structural water is related to changes in the intensity of geopolymer peaks. Figure 13 also depicts the zoomed part of FTIR spectra of geopolymer specimens in the ranges between 900-1200 cm⁻¹, 1500-1800 cm⁻¹, and 3300-3600 cm⁻¹, respectively. Toniolo *et al.* [58] reported that a peak in fly ash at 790 cm⁻¹ and 800 cm⁻¹ indicates the presence of quartz or mullite. Das *et al.* [59] reported that the presence of a symmetric band at 778 cm⁻¹ ascribes to the quartz, which was also reported by other researchers [60,61]. Table 6 displays the presence of various peaks in the fly ash powder and geopolymer specimen ID GP14MAC390D, respectively, along with their possible assignments.

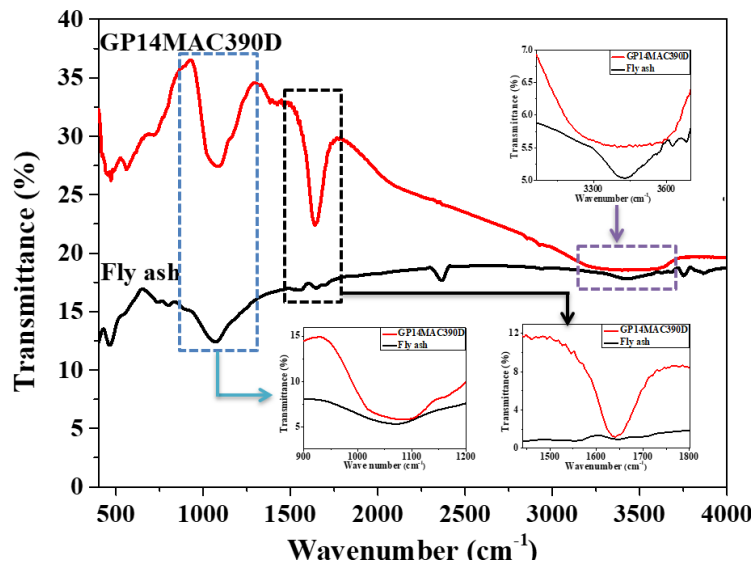


Figure 13. FTIR spectra of fly ash and GP14MAC geopolymer specimen.

Table 6. FTIR wavenumbers and their possible assignments: (a) Fly ash; (b) GP14MAC390D.

(a) Fly ash			(b) GP14MAC390D		
Wave numbers (cm ⁻¹)	Possible assignments	References	Wave numbers (cm ⁻¹)	Possible assignments	References
463	Bending vibration of Si-O-Si (For amorphous silicate).	[56,59, 62-64]	470	Bending vibration of Si-O-Si	[56,63,64]
733	Symmetric stretching vibrations of Si-O-Al		564	Bending vibration of Si-O-Al	[58]
799	Symmetric stretching vibrations of Si-O-Si		725	Symmetric stretching vibrations of Si-O-Al	[65]
1071	Asymmetric stretching vibrations of Si-O-T (T= Tetrahedral Si or Al)		1085	Asymmetric stretching vibrations of Si-O-T (T= Tetrahedral Si or Al)	[56,63,64]
1553	Stretching vibration of (O-C-O)	[66]	1645	Bending vibrations of H-O-H	[56,58]

(a) Fly ash			(b) GP14MAC390D		
Wave numbers (cm ⁻¹)	Possible assignments	References	Wave numbers (cm ⁻¹)	Possible assignments	References
1647	Bending vibrations of H-O-H	[56]	2345	Infrared band position of HCO ₃ ⁻ / stretching vibration of KBr	[67,68]
2355	Infrared band position of HCO ₃ ⁻ / stretching vibration of KBr	[67,68]	3433	Stretching vibrations of OH	[56]
3428-3442	Stretching vibrations of OH	[56]			

X-ray diffraction analysis of fly ash and the geopolymer specimen ID GP14MAC390D was performed to identify the mineralogical characteristics. Figure 14 shows the x-ray diffraction pattern of fly ash powder and the geopolymer specimen id GP14MAC390D, which was cured for 390 days, respectively. In Figure 14, Q and M indicate the quartz and mullite, respectively. The major crystalline peaks that are present in the fly ash are mullite and quartz. The same diffraction pattern and phases are also observed on the fly ash-based geopolymer specimen, which was cured under ambient conditions for 390 days. The broad hump in fly ash ranging between 12°- 31°, indicates the presence of an amorphous phase in the materials. It can also be seen that the hump in geopolymer specimen ID GP14MAC390D is slightly flattened in comparison to the x-ray diffraction pattern of starting raw materials, i.e., fly ash. So, we can conclude that the increase in curing days (390 days) changes the amorphicity slightly but does not change the crystalline phases, which was also observed by Arioz *et al.* [69]. Xie *et al.* [70] reported that the presence of amorphous phases in the geopolymer specimen may be due to the combination of newly formed geopolymer compounds and the unreacted amorphous oxide from the fly ash, respectively. Comparing the peak intensity of both the fly ash and ambient cured geopolymer specimen (GP14MAC390D), it was observed that the intensity of the peaks decreased. Cristelo *et al.* also observed a decrease in the peak intensity [71].

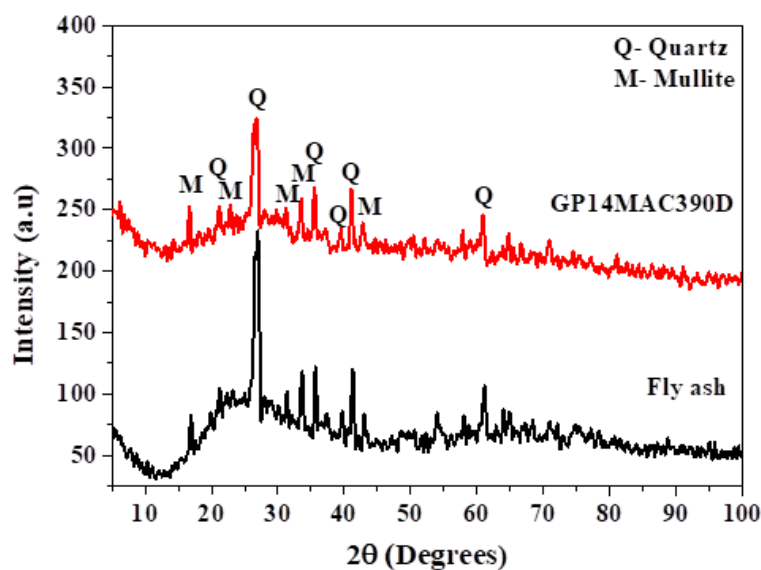


Figure 14. X-ray diffraction pattern of fly ash and the GP14MAC390D geopolymer specimen.

It is crucial to calculate the amount of water absorbed by the geopolymer specimen to examine the geopolymer specimen's resistance to rain penetration. The water absorption

analysis table for the geopolymer specimen with ID GP14MAC390D is displayed in Table 7. The water absorption percentage was calculated using the following formula:

$$\text{Water absorption}(\%) = \frac{(W_w - D_w)}{D_w} \times 100 \quad [72]$$

Where W_w is the wet weight, and D_w is the dry weight of the geopolymer specimen.

Table 7. Water absorption test of geopolymer specimen.

Sl. no.	Geopolymer specimen ID	Curing age (days)	Water absorption (%)			Average water absorption (%)
			Sample no 1	Sample no 2	Sample no 3	
1	GP14MAC390D	7	7.86	7.98	8.24	8.02
2	GP14MAC390D	14	6.56	6.11	6.78	6.48
3	GP14MAC390D	28	5.54	5.87	5.71	5.70

The visual examination revealed that after water absorption, the color of the geopolymer specimen changed from grey to light white. The curing age (days) for geopolymer specimens are 7 days, 14 days, and 28 days, respectively. The geopolymer specimen shows water absorption rates of 8.02 %, 6.48 %, and 5.70 % after water absorption for 7 days, 14 days, and 28 days, respectively. Over time, the reduction in pore size in the geopolymer specimen may account for the decrease in water absorption. The same observation was reported by other researchers also [73,74]. Mastura *et al.* [75] studied the fly ash-based geopolymer bricks where the specimen was water-cured for 1 hour, 6 hours, and 24 hours. A decrease in water absorption was observed with the curing hours, which increased mechanical properties. The increase in strength indicates that the specimen is durable. The fly ash-based geopolymer was studied by Alehyen *et al.* [74], where the water absorption tests of geopolymer paste and ordinary Portland cement paste were conducted for 7, 14, 28, and 90 days. It was observed that with the increase of curing days, the water absorption rate decreased, and the lowest water absorption of 7.2% was achieved with geopolymer paste for 90 days of curing. The decrease in pore size is the main reason for the lowest water absorption, which is related to improving mechanical properties. Thokchom *et al.* [76] studied the durability of fly ash-based geopolymer mortar underwater, where it was observed that the specimen whose water absorption is high shows the lowest compressive strength. The GM3 specimen shows the lowest water absorption of 6.42%, where the maximum residual compressive strength was 54.8%.

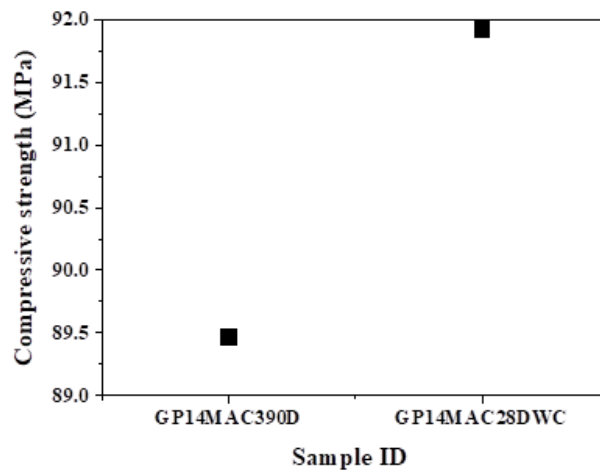


Figure 15. Residual compressive strength of geopolymer specimen.

The residual compressive strength of geopolymer specimen ID GP14MAC390D is tested after the water absorption test, which is shown in Figure 15. After water absorption of

28 days, the specimen ID is changed from GP14MAC390D to GP14MAC28DWC for better understanding. It was observed that the geopolymer specimen, which was ambient cured for 390 days, showed a compressive strength of 89.47 MPa, but after water absorption of 28 days, the specimen ID GP14MAC28DWC showed residual compressive strength of 91.92 MPa. The reduction of pore size may result from the residual compressive strength.

Figure 16 (a-b) shows the SEM fractograph images, and Figure 16 (c) shows the EDS analysis of the geopolymer specimen after immersion in water for 28 days. Visual inspection reveals that specimens undergo a color change from grey to light white after being submerged in water, although the geopolymer specimens are structurally unaltered. Cevik *et al.* [77] also observed the change of color in geopolymer specimens after water absorption. From Figure 16(a-b), it is evident that pores are present in geopolymer specimens, which are further related to the water absorption of the specimens. The reduction of pore size is the main reason for decreased water absorption with curing time. The EDS analysis of geopolymer specimen ID GP14MAC390D shows the formation of N-A-S-H gel, and its presence indicates that the specimens are structurally unaltered.

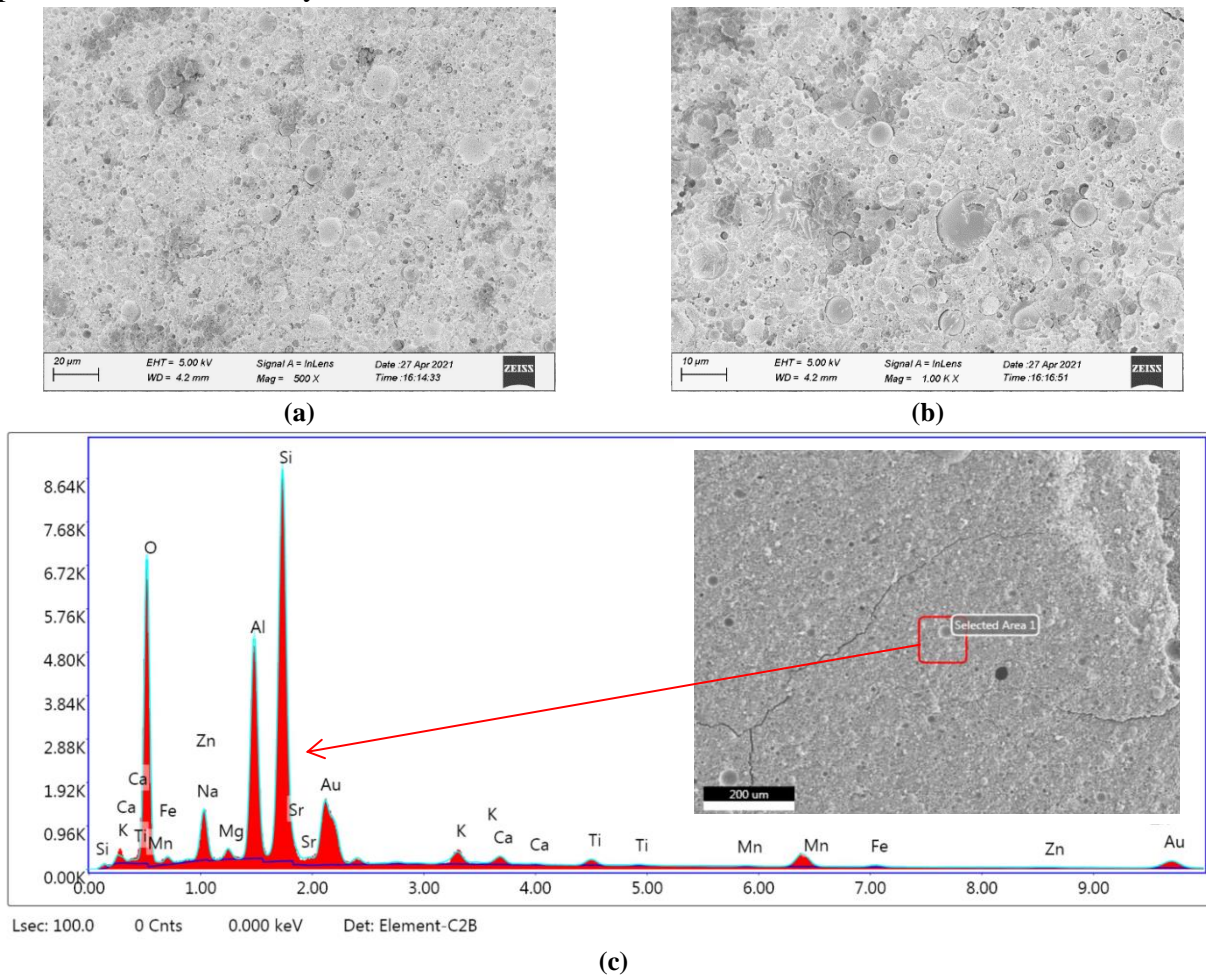


Figure 16. (a-b) SEM fractograph images; (c) EDS analysis of geopolymer specimen after immersion in water for 28 days.

4. Conclusions

The fly ash-based geopolymer specimens cured under ambient conditions are studied. After testing and characterizations, the following conclusions are drawn: the compressive strength of geopolymer specimen ID GP14MAC is enhanced by the curing time (days); therefore, the curing process and the length of the curing time are crucial; the highest

compressive strength flexural strength, and Vickers microhardness value of 89.47 MPa, 15.8 MPa, and 171.21 HV is achieved with the geopolymer specimen cured for 390 days under ambient curing conditions; the major reaction product, which is primarily accountable for the growth of mechanical strength, is the production of sodium aluminosilicate gel. FESEM analysis of fractured geopolymer specimens cured for 390 days shows that most of the particles are diffused due to high alkaline activation as compared to the geopolymer specimen cured for 3 days only. EDS analysis also confirms the formation of sodium aluminosilicate gel; the FTIR analysis confirms the formation of new reaction products by shifting the asymmetric stretching vibrations of Si-O-T (T= Tetrahedral Si or Al) in the geopolymer specimen compared to the starting raw materials; the ambient cured geopolymer specimen ID GP14MAC (390 days) shows the lowest water absorption of 5.70% with the curing age (days) of 28 days. The geopolymer specimen ID GP14MAC390D (390 days) shows a residual compressive strength of 91.92 MPa after water absorption of 28 days.

Funding

The work has received financial support from Govind Ballabh Pant National Institute of Himalayan Environment and Sustainable Development (IERP Project), Government of India, for funding the research project entitled “Production of Geopolymer based construction material from Fly ash: An industrial waste.” bearing grant no: GBPI/IERP/17-18/44 dated 28th March 2018.

Acknowledgments

The authors would like to thank the Central Instrumentation Center, Tripura University (A Central University), Agartala, Tripura, India, and the Department of Chemical and Polymer Engineering, Tripura University, Agartala, for the FESEM and FTIR facility.

Conflicts of Interest

The authors declare no conflict of interest.

References

1. Das, D.; Rout, P.K. A Review of Coal Fly Ash Utilization to Save the Environment. *Water, Air, Soil Pollut.* **2023**, *234*, 128, doi:10.1007/s11270-023-06143-9.
2. Liu, H.; Liu, Y.; Duan, P.; Bian, H.; Wang, K.; Lou, J.; Zhang, H.; Ge, Z. Design and Optimization of Binary Geopolymers Derived from Red Mud-Coal Gasification Slag Based on Response Surface Methodology. *Constr. Build. Mater.* **2025**, *464*, 140203, doi:10.1016/j.conbuildmat.2025.140203.
3. Das, D.; Das, A.P.; Rout, P.K. Effect of Slag Addition on Compressive Strength and Microstructural Features of Fly Ash Based Geopolymer. In *Circular Economy in the Construction Industry*; CRC Press: Boca Raton, **2021**; pp. 61–68.
4. Sarkar, C.; Basu, J.K.; Samanta, A.N. Experimental and Kinetic Study of Fluoride Adsorption by Ni and Zn Modified LD Slag Based Geopolymer. *Chem. Eng. Res. Des.* **2019**, *142*, 165–175, doi:10.1016/j.cherd.2018.12.006.
5. Nath, S.K. Fly Ash and Zinc Slag Blended Geopolymer: Immobilization of Hazardous Materials and Development of Paving Blocks. *J. Hazard. Mater.* **2020**, *387*, 121673, doi:10.1016/j.jhazmat.2019.121673.
6. Luo, Z.; Zhi, T.; Liu, L.; Mi, J.; Zhang, M.; Tian, C.; Si, Z.; Liu, X.; Mu, Y. Solidification/Stabilization of Chromium Slag in Red Mud-Based Geopolymer. *Constr. Build. Mater.* **2022**, *316*, 125813, doi:10.1016/j.conbuildmat.2021.125813.
7. Yu, S.; Zhao, W.; Li, H.; Guo, R.; Guo, H. Green Transformation of Ferrochrome Slag by Geopolymers: Physical Properties, Fly Ash Replacement and Chromium Immobilization. *Constr. Build. Mater.* **2025**, *462*, 140063, doi:10.1016/j.conbuildmat.2025.140063.
8. Wu, Y.; Wang, M.; Sun, Z.; Zhang, D. High Temperature Performance of High Magnesium Nickel Slag

- Based Geopolymers with Different P/Al Molar Ratios Prepared by Acidic Activator. *Case Stud. Constr. Mater.* **2024**, *20*, e03275, doi:10.1016/j.cscm.2024.e03275.
9. 2018 BP Energy Outlook. **2018**, 125. <https://www.bp.com/content/dam/bp/en/corporate/pdf/energy-economics/energy-outlook/bp-energy-outlook-2018.pdf>
 10. Bhattacharyya, S.; Donahoe, R.J.; Patel, D. Experimental Study of Chemical Treatment of Coal Fly Ash to Reduce the Mobility of Priority Trace Elements. *Fuel* **2009**, *88*, 1173–1184, doi:10.1016/j.fuel.2007.11.006.
 11. Das, D.; Rout, P.K. Coal Fly Ash Utilization in India. In *New Horizons for Industry 4.0 in Modern Business*; Nayyar, A., Naved, M., Rameshwar, R., Eds.; Springer, Cham, **2023**; pp. 233–251 ISBN 978-3-031-20443-2.
 12. Sall, M.; Dieye, G.; Traoré, A.; Gueye, P.M.; Diouf, S.; Wade, A.C.; Diop, D. Technological and Environmental Behavior of Coal Fly Ash in Lime-Based Materials. *Geomaterials* **2022**, *12*, 15–29, doi:10.4236/gm.2022.122002.
 13. Das, D.; Gołabiewska, A.; Rout, P.K. Geopolymer Bricks: The next Generation of Construction Materials for Sustainable Environment. *Constr. Build. Mater.* **2024**, *445*, 137876, doi:10.1016/j.conbuildmat.2024.137876.
 14. Das, D. Role of Particle Size on the Mechanical and Microstructural Properties of Fly Ash-Based Geopolymer. *Interactions* **2024**, *245*, 277, doi:10.1007/s10751-024-02117-3.
 15. Roy, R.; Das, D.; Rout, P.K. A Review of Advanced Mullite Ceramics. *Eng. Sci.* **2022**, *18*, 20–30, doi:10.30919/es8d582.
 16. Roy, R.; Das, D.; Rout, P.K. Fabrication of Mullite Ceramic by Using Industrial Waste. In *Smart Cities*; CRC Press: Boca Raton, **2022**; pp. 285–291.
 17. Xu, H.; Van Deventer, J.S.J. The Geopolymerisation of Alumino-Silicate Minerals. *Int. J. Miner. Process.* **2000**, *59*, 247–266, doi:10.1016/S0301-7516(99)00074-5.
 18. Venkatesan, G.; Alengaram, U.J.; Ibrahim, S.; Ibrahim, M.S.I. Effect of Fly Ash Characteristics, Sodium-Based Alkaline Activators, and Process Variables on the Compressive Strength of Siliceous Fly Ash Geopolymers with Microstructural Properties: A Comprehensive Review. *Constr. Build. Mater.* **2024**, *437*, 136808, doi:10.1016/j.conbuildmat.2024.136808.
 19. Xiao, Q.; Tang, Z.; Xiang, Y.; Cai, Y.; Wang, J.; Xu, W.; Long, G. Early Age Reaction, Rheological Properties, and Environment Impact of NaOH-Activated Fly Ash Mixtures at Ambient Environment. *J. Build. Eng.* **2024**, *88*, 109145, doi:10.1016/j.job.2024.109145.
 20. Rahman, S.K.; Al-Ameri, R. A Newly Developed Self-Compacting Geopolymer Concrete under Ambient Condition. *Constr. Build. Mater.* **2021**, *267*, 121822, doi:10.1016/j.conbuildmat.2020.121822.
 21. Verma, M.; Dev, N. Sodium Hydroxide Effect on the Mechanical Properties of Flyash-Slag Based Geopolymer Concrete. *Struct. Concr.* **2020**, 1–12, doi:10.1002/suco.202000068.
 22. Somna, K.; Jaturapitakkul, C.; Kajitvichyanukul, P.; Chindaprasirt, P. NaOH-Activated Ground Fly Ash Geopolymer Cured at Ambient Temperature. *Fuel* **2011**, *90*, 2118–2124, doi:10.1016/j.fuel.2011.01.018.
 23. Rajesh, A.M. Study of the Strength Geopolymer Concrete with Alkaline Solution of Varying Molarity. *IOSR J. Eng.* **2014**, *4*, 19–24, doi:10.9790/3021-04611924.
 24. Mudgal, M.; Singh, A.; Chouhan, R.K.; Acharya, A.; Srivastava, A.K. Fly Ash Red Mud Geopolymer with Improved Mechanical Strength. *Clean. Eng. Technol.* **2021**, *4*, 100215, doi:10.1016/j.clet.2021.100215.
 25. Masi, G.; Filipponi, A.; Bignozzi, M.C. Fly Ash-Based One-Part Alkali Activated Mortars Cured at Room Temperature: Effect of Precursor Pre-Treatments. *Open Ceram.* **2021**, *8*, 100178, doi:10.1016/j.oceram.2021.100178.
 26. Bhavsar, J.K.; Panchal, V. Ceramic Waste Powder as a Partial Substitute of Fly Ash for Geopolymer Concrete Cured at Ambient Temperature. *Civ. Eng. J.* **2022**, *8*, 1369–1387, doi:10.28991/CEJ-2022-08-07-05.
 27. Niş, A.; Altındal, İ. Compressive Strength Performance of Alkali Activated Concretes under Different Curing Conditions. *Period. Polytech. Civ. Eng.* **2021**, doi:10.3311/PPci.17016.
 28. Das, D.; Rout, P.K. Synthesis, Characterization and Properties of Fly Ash Based Geopolymer Materials. *J. Mater. Eng. Perform.* **2021**, *30*, 3213–3231, doi:10.1007/s11665-021-05647-x.
 29. Turkey, F.A.; Beddu, S.B.; Ahmed, A.N.; Al-Hubboubi, S.K. Effect of High Temperatures on the Properties of Lightweight Geopolymer Concrete Based Fly Ash and Glass Powder Mixtures. *Case Stud. Constr. Mater.* **2022**, *17*, e01489, doi:10.1016/j.cscm.2022.e01489.
 30. Debnath, K.; Das, D.; Kumar Rout, P. Effect of Mechanical Milling of Fly Ash Powder on Compressive Strength of Geopolymer. *Mater. Today Proc.* **2022**, *68*, 242–249, doi:10.1016/j.matpr.2022.08.321.
 31. Suraneni, P.; Burriss, L.; Shearer, C.R.; Hooton, R.D. ASTM C618 Fly Ash Specification: Comparison with Other Specifications, Shortcomings, and Solutions. *ACI Mater. J.* **2021**, *118*, 157–167, doi:10.14359/51725994.
 32. Khairul Nizar, I.; Al Bakri, A.M.M.; Rafiza, A.R.; Kamarudin, H.; Abdullah, A.; Yahya, Z. Study on Physical and Chemical Properties of Fly Ash from Different Area in Malaysia. *Key Eng. Mater.* **2013**, *594–595*, 985–989, doi:10.4028/www.scientific.net/KEM.594-595.985.
 33. Wang, C.; Kayali, O.; Liow, J.-L. The Effectiveness and Mechanisms of Superplasticisers in Dispersing Class F Fly Ash Pastes. *Powder Technol.* **2021**, *392*, 81–92, doi:10.1016/j.powtec.2021.06.054.

34. Rivera, J.F.; Orobio, A.; Cristelo, N.; Mejía de Gutiérrez, R. Fly Ash-Based Geopolymer as A4 Type Soil Stabiliser. *Transp. Geotech.* **2020**, *25*, 100409, doi:10.1016/j.trgeo.2020.100409.
35. Diaz, E.I.; Allouche, E.N.; Eklund, S. Factors Affecting the Suitability of Fly Ash as Source Material for Geopolymers. *Fuel* **2010**, *89*, 992–996, doi:10.1016/j.fuel.2009.09.012.
36. Szabó, R.; Dolgos, F.; Debreczeni, Á.; Mucsi, G. Scale-up Experiments of Expanded Perlite-Geopolymer Composite Block with Special Regard to the Effect of Water. *Constr. Build. Mater.* **2025**, *464*, 140166, doi:10.1016/j.conbuildmat.2025.140166.
37. Cai, J.; Li, X.; Tan, J.; Vandevyvere, B. Thermal and Compressive Behaviors of Fly Ash and Metakaolin-Based Geopolymer. *J. Build. Eng.* **2020**, *30*, 101307, doi:10.1016/j.job.2020.101307.
38. Nath, P.; Sarker, P.K. Fracture Properties of GGBFS-Blended Fly Ash Geopolymer Concrete Cured in Ambient Temperature. *Mater. Struct.* **2017**, *50*, 32, doi:10.1617/s11527-016-0893-6.
39. Vijai, K.; Kumutha, R.; Vishnuram, B.G. Effect of Types of Curing on Strength of Geopolymer Concrete. *Int. J. Phys. Sci.* **2010**, *5*, 1419–1423.
40. Hassan, A.; Arif, M.; Shariq, M. Effect of Curing Condition on the Mechanical Properties of Fly Ash-Based Geopolymer Concrete. *SN Appl. Sci.* **2019**, *1*, doi:10.1007/s42452-019-1774-8.
41. Shekhawat, P.; Sharma, G.; Martand, R. Strength Behavior of Alkaline Activated Eggshell Powder and Flyash Geopolymer Cured at Ambient Temperature. *Constr. Build. Mater.* **2019**, *223*, 1112–1122, doi:10.1016/j.conbuildmat.2019.07.325.
42. Diamond, S. Particle Morphologies in Fly Ash. *Cem. Concr. Res.* **1986**, *16*, 569–579, doi:10.1016/0008-8846(86)90095-5.
43. Fernández-Jiménez, A.; Palomo, A. Composition and Microstructure of Alkali Activated Fly Ash Binder: Effect of the Activator. *Cem. Concr. Res.* **2005**, *35*, 1984–1992, doi:10.1016/j.cemconres.2005.03.003.
44. Ambikakumari Sanalkumar, K.U.; Lahoti, M.; Yang, E.H. Investigating the Potential Reactivity of Fly Ash for Geopolymerization. *Constr. Build. Mater.* **2019**, *225*, 283–291, doi:10.1016/j.conbuildmat.2019.07.140.
45. Steveson, M.; Sagoe-Crentsil, K. Relationships between Composition, Structure and Strength of Inorganic Polymers. *J. Mater. Sci.* **2005**, *40*, 2023–2036, doi:10.1007/s10853-005-1226-2.
46. Lyngdoh, G.A.; Nayak, S.; Krishnan, N.M.A.; Das, S. Fracture Toughness of Fly Ash-Based Geopolymer Gels: Evaluations Using Nanoindentation Experiment and Molecular Dynamics Simulation. *Constr. Build. Mater.* **2020**, *262*, 120797, doi:10.1016/j.conbuildmat.2020.120797.
47. Luo, Z.; Li, W.; Li, P.; Wang, K.; Shah, S.P. Investigation on Effect of Nanosilica Dispersion on the Properties and Microstructures of Fly Ash-Based Geopolymer Composite. *Constr. Build. Mater.* **2021**, *282*, 122690, doi:10.1016/j.conbuildmat.2021.122690.
48. Öz, H.Ö.; Yücel, H.E.; Güneş, M.; Köker, T.Ş. Fly-Ash-Based Geopolymer Composites Incorporating Cold-Bonded Lightweight Fly Ash Aggregates. *Constr. Build. Mater.* **2021**, *272*, 121963, doi:10.1016/j.conbuildmat.2020.121963.
49. Azimi, E.A.; Abdullah, M.M.A.B.; Vizureanu, P.; Salleh, M.A.A.M.; Sandu, A.V.; Chairapa, J.; Yoriya, S.; Hussin, K.; Aziz, I.H. Strength Development and Elemental Distribution of Dolomite/Fly Ash Geopolymer Composite under Elevated Temperature. *Materials (Basel)*. **2020**, *13*, 1015, doi:10.3390/ma13041015.
50. Kränzlein, E.; Pöllmann, H.; Krcmar, W. Metal Powders as Foaming Agents in Fly Ash Based Geopolymer Synthesis and Their Impact on the Structure Depending on the Na /Al Ratio. *Cem. Concr. Compos.* **2018**, *90*, 161–168, doi:10.1016/j.cemconcomp.2018.02.009.
51. Shekhawat, P.; Sharma, G.; Singh, R.M. Microstructural and Morphological Development of Eggshell Powder and Flyash-Based Geopolymers. *Constr. Build. Mater.* **2020**, *260*, 119886, doi:10.1016/j.conbuildmat.2020.119886.
52. Kumar, A.; Kumar, S. Development of Paving Blocks from Synergistic Use of Red Mud and Fly Ash Using Geopolymerization. *Constr. Build. Mater.* **2013**, *38*, 865–871, doi:10.1016/j.conbuildmat.2012.09.013.
53. Chithambaram, S.J.; Kumar, S.; Prasad, M.M. Thermo-Mechanical Characteristics of Geopolymer Mortar. *Constr. Build. Mater.* **2019**, *213*, 100–108, doi:10.1016/j.conbuildmat.2019.04.051.
54. Nath, S.K.; Kumar, S. Role of Particle Fineness on Engineering Properties and Microstructure of Fly Ash Derived Geopolymer. *Constr. Build. Mater.* **2020**, *233*, 117294, doi:10.1016/j.conbuildmat.2019.117294.
55. Pu, S.; Zhu, Z.; Song, W.; Huo, W.; Zhang, J. Mechanical and Microscopic Properties of Fly Ash Phosphoric Acid-Based Geopolymer Paste: A Comprehensive Study. *Constr. Build. Mater.* **2021**, *299*, 123947, doi:10.1016/j.conbuildmat.2021.123947.
56. Rožek, P.; Król, M.; Mozgawa, W. Spectroscopic Studies of Fly Ash-Based Geopolymers. *Spectrochim. Acta - Part A Mol. Biomol. Spectrosc.* **2018**, *198*, 283–289, doi:10.1016/j.saa.2018.03.034.
57. Cheng, X.; Tang, X.; Huang, F. Synthesis and Characterization of Novel Fluorosilicone Triblock Copolymers. *IOP Conf. Ser. Mater. Sci. Eng.* **2020**, *774*, 012012, doi:10.1088/1757-899X/774/1/012012.
58. Toniolo, N.; Taveri, G.; Hurle, K.; Roether, J.A.; Ercole, P.; Dlouhý, I.; Boccaccini, A.R. Fly-Ash-Based Geopolymers: How the Addition of Recycled Glass or Red Mud Waste Influences the Structural and Mechanical Properties. *J. Ceram. Sci. Technol.* **2017**, *8*, 411–419, doi:10.4416/JCST2017-00053.
59. Das, D.; Rout, P.K. Synthesis of Inorganic Polymeric Materials from Industrial Solid Waste. *Silicon* **2022**, *15*, 1771–1791, doi:10.1007/s12633-022-02116-5.

60. Sukmak, P.; Kunchariyakun, K.; Sukmak, G.; Horpibulsuk, S.; Kassawat, S.; Arulrajah, A. Strength and Microstructure of Palm Oil Fuel Ash-Fly Ash-Soft Soil Geopolymer Masonry Units. *J. Mater. Civ. Eng.* **2019**, *31*, 1–13, doi:10.1061/(ASCE)MT.1943-5533.0002809.
61. Ismail, I.; Bernal, S.A.; Provis, J.L.; San Nicolas, R.; Hamdan, S.; Van Deventer, J.S.J. Modification of Phase Evolution in Alkali-Activated Blast Furnace Slag by the Incorporation of Fly Ash. *Cem. Concr. Compos.* **2014**, *45*, 125–135, doi:10.1016/j.cemconcomp.2013.09.006.
62. Das, D.; Rout, P.K. Utilization of Thermal Industry Waste: From Trash to Cash. *Carbon – Sci. Technol.* **2019**, *11*, 43–48.
63. Lee, W.K.W.; Van Deventer, J.S.J. Use of Infrared Spectroscopy to Study Geopolymerization of Heterogeneous Amorphous Aluminosilicates. *Langmuir* **2003**, *19*, 8726–8734, doi:10.1021/la026127e.
64. Jang, J.G.; Lee, H.K. Effect of Fly Ash Characteristics on Delayed High-Strength Development of Geopolymers. *Constr. Build. Mater.* **2016**, *102*, 260–269, doi:10.1016/j.conbuildmat.2015.10.172.
65. Zhang, X.; Zhang, X.; Li, X.; Tian, D.; Ma, M.; Wang, T. Optimized Pore Structure and High Permeability of Metakaolin/Fly-Ash-Based Geopolymer Foams from Al- and H₂O₂-Sodium Oleate Foaming Systems. *Ceram. Int.* **2022**, *48*, 18348–18360, doi:10.1016/j.ceramint.2022.03.094.
66. Lee, W.K.W.; van Deventer, J.S.J. The Effects of Inorganic Salt Contamination on the Strength and Durability of Geopolymers. *Colloids Surfaces A Physicochem. Eng. Asp.* **2002**, *211*, 115–126, doi:10.1016/S0927-7757(02)00239-X.
67. Kumar, S.; Kristály, F.; Mucsi, G. Geopolymerisation Behaviour of Size Fractioned Fly Ash. *Adv. Powder Technol.* **2015**, *26*, 24–30, doi:10.1016/j.apt.2014.09.001.
68. Khater, H.M.; El Naggar, A. Combination between Organic Polymer and Geopolymer for Production of Eco-Friendly Metakaolin Composite. *J. Aust. Ceram. Soc.* **2020**, *56*, 599–608, doi:10.1007/s41779-019-00371-1.
69. Arioiz, E.; Arioiz, O.; Kockar, O.M. Geopolymer Synthesis with Low Sodium Hydroxide Concentration. *Iran. J. Sci. Technol. - Trans. Civ. Eng.* **2020**, *2*–10, doi:10.1007/s40996-019-00336-1.
70. Xie, J.; Kayali, O. Effect of Initial Water Content and Curing Moisture Conditions on the Development of Fly Ash-Based Geopolymers in Heat and Ambient Temperature. *Constr. Build. Mater.* **2014**, *67*, 20–28, doi:10.1016/j.conbuildmat.2013.10.047.
71. Cristelo, N.; Glendinning, S.; Fernandes, L.; Pinto, A.T. Effect of Calcium Content on Soil Stabilisation with Alkaline Activation. *Constr. Build. Mater.* **2012**, *29*, 167–174, doi:10.1016/j.conbuildmat.2011.10.049.
72. Mehta, A.; Siddique, R. Properties of Low-Calcium Fly Ash Based Geopolymer Concrete Incorporating OPC as Partial Replacement of Fly Ash. *Constr. Build. Mater.* **2017**, *150*, 792–807, doi:10.1016/j.conbuildmat.2017.06.067.
73. Razak, S.; Zainal, F.F.; Shamsudin, S.R. Effect of Porosity and Water Absorption on Compressive Strength of Fly Ash Based Geopolymer and OPC Paste. *IOP Conf. Ser. Mater. Sci. Eng.* **2020**, *957*, 012035, doi:10.1088/1757-899X/957/1/012035.
74. Alehyen, S.; Achouri, M.E.L.; Taibi, M. Characterization , Microstructure and Properties of Fly Ash-Based Geopolymer. **2017**, *8*, 1783–1796.
75. Wan Mastura, W.I.; Kamarudin, H.; Khairul Nizar, I.; Al Bakri Abdullah, M.M.; Mohammed, H. The Effect of Curing Time on the Properties of Fly Ash-Based Geopolymer Bricks. *Adv. Mater. Res.* **2012**, *626*, 937–941, doi:10.4028/www.scientific.net/AMR.626.937.
76. Thokchom, S.; Ghosh, P.; Ghosh, S. Effect of Water Absorption, Porosity and Sorptivity on Durability of Geopolymer Mortars. *J. Eng. Appl. Sci.* **2009**, *4*, 28–32.
77. Çevik, A.; Alzeebaree, R.; Humur, G.; Niş, A.; Gülşan, M.E. Effect of Nano-Silica on the Chemical Durability and Mechanical Performance of Fly Ash Based Geopolymer Concrete. *Ceram. Int.* **2018**, *44*, 12253–12264, doi:10.1016/j.ceramint.2018.04.009.